



Original article

A robust luminescent assay for screening alkyladenine DNA glycosylase inhibitors to overcome DNA repair and temozolomide drug resistance



Ying-Qi Song^a, Guo-Dong Li^a, Dou Niu^a, Feng Chen^a, Shaozhen Jing^c,
Vincent Kam Wai Wong^d, Wanhe Wang^{c,*}, Chung-Hang Leung^{a,b,**}

^a State Key Laboratory of Quality Research in Chinese Medicine, Institute of Chinese Medical Sciences, University of Macau, Macao, 999078, China

^b Department of Biomedical Sciences, Faculty of Health Sciences, University of Macau, Macao, 999078, China

^c Institute of Medical Research, Northwestern Polytechnical University, Xi'an, 710072, China

^d Dr. Neher's Biophysics Laboratory for Innovative Drug Discovery, State Key Laboratory of Quality Research in Chinese Medicine, Macau University of Science and Technology, Macao, 999078, China

ARTICLE INFO

Article history:

Received 6 January 2023

Received in revised form

22 March 2023

Accepted 15 April 2023

Available online 19 April 2023

Keywords:

Drug screening

Alkyladenine DNA glycosylase

N³-methyladenine

Glioblastoma

Temozolomide

Sunitinib

ABSTRACT

Temozolomide (TMZ) is an anticancer agent used to treat glioblastoma, typically following radiation therapy and/or surgical resection. However, despite its effectiveness, at least 50% of patients do not respond to TMZ, which is associated with repair and/or tolerance of TMZ-induced DNA lesions. Studies have demonstrated that alkyladenine DNA glycosylase (AAG), an enzyme that triggers the base excision repair (BER) pathway by excising TMZ-induced N³-methyladenine (3meA) and N⁷-methylguanine lesions, is overexpressed in glioblastoma tissues compared to normal tissues. Therefore, it is essential to develop a rapid and efficient screening method for AAG inhibitors to overcome TMZ resistance in glioblastomas. Herein, we report a robust time-resolved photoluminescence platform for identifying AAG inhibitors with improved sensitivity compared to conventional steady-state spectroscopic methods. As a proof-of-concept, this assay was used to screen 1440 food and drug administration-approved drugs against AAG, resulting in the repurposing of sunitinib as a potential AAG inhibitor. Sunitinib restored glioblastoma (GBM) cancer cell sensitivity to TMZ, inhibited GBM cell proliferation and stem cell characteristics, and induced GBM cell cycle arrest. Overall, this strategy offers a new method for the rapid identification of small-molecule inhibitors of BER enzyme activities that can prevent false negatives due to a fluorescent background.

© 2023 The Authors. Published by Elsevier B.V. on behalf of Xi'an Jiaotong University. This is an open access article under the CC BY-NC-ND license (<http://creativecommons.org/licenses/by-nc-nd/4.0/>).

1. Introduction

Glioblastoma, also referred to as glioblastoma (GBM), is an aggressive type of brain cancer. The standard treatment for GBM involves surgical intervention, followed by radiotherapy and chemotherapy. Temozolomide (TMZ) is a first-line therapy for treating GBM. TMZ induces the formation of the methyl adducts N⁷-methylguanine, O⁶-methylguanine, and N³-methyladenine in the DNA, ultimately resulting in apoptosis [1]. Although chemotherapy

can extend postoperative survival, it has been observed that at least 50% of patients ultimately do not respond to TMZ [2].

Most DNA base adducts induced by TMZ are fixed by the base excision repair (BER) pathway; thus, inhibition of this pathway can increase sensitivity to anticancer drugs [3]. Alkyladenine DNA glycosylase (AAG, alternatively called alkyl-N-purine glycosylase, and N-methylpurine-DNA glycosylase) is a type of BER enzyme [4]. AAG recognizes and excises damaged bases from DNA after alkylation or oxidative DNA damage, generating an apurinic (AP) site [5]. Then, AAG recruits apurinic/aprimidinic endonuclease 1 (APE1) to the abasic site, which cleaves the DNA backbone to reveal a single-strand break with 3'-OH and 5'-deoxyribose phosphate (dRP) termini. Subsequently, DNA polymerase β removes the 5e-dRP to reveal a single nucleotide gap, in which DNA ligase seals after DNA polymerase β has filled it. Overexpression of AAG is linked to an increased risk of lung cancer and colorectal cancer [6,7], and

Peer review under responsibility of Xi'an Jiaotong University.

* Corresponding author.

** Corresponding author. State Key Laboratory of Quality Research in Chinese Medicine, Institute of Chinese Medical Sciences, University of Macau, 999078, Macao, China.

E-mail addresses: whwang0206@nwpu.edu.cn (W. Wang), duncanleung@um.edu.mo (C.-H. Leung).

<https://doi.org/10.1016/j.jpha.2023.04.010>

2095-1779/© 2023 The Authors. Published by Elsevier B.V. on behalf of Xi'an Jiaotong University. This is an open access article under the CC BY-NC-ND license (<http://creativecommons.org/licenses/by-nc-nd/4.0/>).

decreased patient survival in malignant GBM [8]. Several studies have also demonstrated that AAG increases drug resistance in various types of cancers [9,10]. Downregulation of AAG in HeLa and ovarian cancer cells increased the potency of TMZ and *N*-methyl-*N*-nitrosourea [5]. Therefore, AAG is a potential target for cancer treatments, including GBM.

Gel electrophoresis in conjunction with radioactive labeling is considered the “gold standard” for assessing the activity of DNA-modifying enzymes [11]. Although other techniques such as bioinformatics, fragment-substrate tethering, radioisotopic labeling, affinity chromatography, and chemical cross-linking have been reported for measuring DNA-modifying enzyme activity, they often have drawbacks such as being time-consuming, complex, and/or requiring strict safety protocols to minimize exposure to radiation. Thus, novel in vitro methods that can rapidly and efficiently identify AAG inhibitors are urgently required. Fluorescence methods using organic dyes have been developed to monitor DNA repair enzyme activities [12,13]. However, the fluorescence of organic dyes has a short lifetime in the nanosecond range, which makes it difficult to distinguish their signal from the high background fluorescence of the samples. This can lead to false negatives, thus limiting the use of organic dyes in drug screening applications.

Luminescent transition metal complexes, such as iridium (III) complexes, exhibit higher quantum yields than organic dyes [14]. Moreover, in contrast to the limited range of emission wavelengths of ruthenium (II) complexes, iridium (III) complexes can be fine-tuned to display a variety of emission colors by modifying the included ligands [14,15]. Meanwhile, the use of iridium (III) complexes in time-resolved emission spectroscopy (TRES) can circumvent the issue of background autofluorescence owing to their long phosphorescent lifetimes and significant Stokes shift values (usually exceeding 120 nm) [16]. A number of iridium (III) complexes have been described for drug screening [16–19], and some iridium (III) complexes have been designed and used as selective G-quadruplex selectivity probes in our previous study [16,20,21].

The G-quadruplex is a non-canonical DNA secondary structure formed by guanine-rich sequences [22]. Owing to its tremendous structural diversity, the G-quadruplex structure has been utilized for several in vitro applications, including analytical assays [23–27]. Moreover, G-quadruplexes have been identified as effective signal-transducing units for the development of G-quadruplex-based sensing assays [28]. In a typical G-quadruplex-based sensing platform, the presence of an analyte causes a specific DNA sequence, often in the ssDNA or dsDNA form, to conformationally transition into a G-quadruplex structure [29]. The G-quadruplex probe can then be used to convert the conformational shift of the chosen DNA sequence into a luminescent response [30]. Compared to other DNA structures, a variety of iridium (III) and ruthenium (II) complexes exhibit strong selectivity for G-quadruplex patterns [17,31,32]. With the addition of G-quadruplex DNA, Iridium probes display significant fluorescence amplification [33].

In this study, we report a method for screening AAG inhibitors that combines a long-lived G-quadruplex-selective iridium (III) complex with TRES and DNA-switching strategies. As a proof-of-concept, this assay was used to screen for potential AAG inhibitors in a library containing 1440 US Food and Drug Administration (FDA)-approved drugs. This eventually led to the identification of sunitinib as an AAG inhibitor in GBM.

2. Experimental

2.1. Cell lines and reagents

T98G cells were cultured in Dulbecco's modified Eagle's medium at 37 °C with 5% CO₂, 10% fetal bovine serum, and 1% penicillin/

streptomycin. Sunitinib, morin, and TMZ were purchased from MedChemExpress Ltd. (MCE, Monmouth Junction, NJ, USA) and dissolved in 10 mM dimethyl sulfoxide (DMSO). Oligonucleotides were synthesized by IGE Bio Inc. (Guangzhou, China) and the BGI group (Shenzhen, China). Related sequences are listed in Table S1. The probe (Fig. S1) was synthesized as described in our previous study [19].

2.2. Screening AAG inhibitor

A solution containing 100 μM of F1 and R1 sequences in a solution of 150 mM NaCl, 50 mM Tris, and pH 7.0 was subjected to incubation at 95 °C for 10 min. Following this, the solution was cooled to 4 °C to facilitate the formation of the duplex substrate (F1–R1). F1–R1 was then incubated with appropriate concentrations of AAG, APE1, and US FDA-approved drugs (10 μM). The mixture solution was incubated at 37 °C for 30 min and then diluted with buffer (25 mM KCl, 50 mM Tris, pH 7.0) to 500 μL. The final concentration of the probe was 1 μM. A HORIBA Fluorolog-3 spectrophotometer (HORIBA–Jobin Yvon, Edison, NJ, USA) was used to obtain steady-state photoluminescence spectra at an excitation wavelength of 355 nm. Time-resolved experiments were performed using the time-correlated single-photon counting technique. The short-lived fluorescence of the potential compounds was eliminated using a 500 ns delay period, while the probe's long-lived phosphorescence was still detectable. The samples were excited at 355 nm and the emission was monitored at 450–700 nm.

2.3. Statistical analysis

Statistical analyses were performed using GraphPad Prism, and the statistical significance was determined using the Student's *t*-test with two groups. Comparisons between three or more groups were analyzed using analysis of variance (ANOVA). *P* values were 2-tailed, and significance was defined as *P* < 0.05. The error bars on the graph show the scanning electron microscopy (SEM) results obtained from three separate experiments.

3. Results

3.1. Design principle of AAG inhibitor screening method

The mechanism of the assay involves the formation of a double-stranded DNA substrate, wherein a G-quadruplex sequence containing 3meA (F1:5'-GTGGGTAGGGCGGGTTGG3meAACTGCGTC-GACCTG-3') partially hybridizes to a complementary DNA strand (R1:3'-CCCAACCTTGACGCAGCTGGAC-5') (Fig. 1). In the presence of AAG, the 3meA lesion was excised to create an AP site on F1. The AP site was subsequently cleaved by APE1, weakening the interaction between F1 and R1 and liberating the G-quadruplex-forming part of F1. The G-quadruplex-forming sequence can reorganize into a G-quadruplex conformation, which can then be detected by the G-quadruplex-selective iridium (III) complex. This interaction results in a significant increase in the emissive response of the iridium (III) complex. However, in the presence of the AAG inhibitor, the liberation of F1 was inhibited, and the luminescence of the iridium (III) complex remained low. The utilization of iridium (III) probes with significant Stokes shifts and extended phosphorescence lifetimes facilitated the detection of their signals using TRES, even in samples with high levels of fluorescent background.

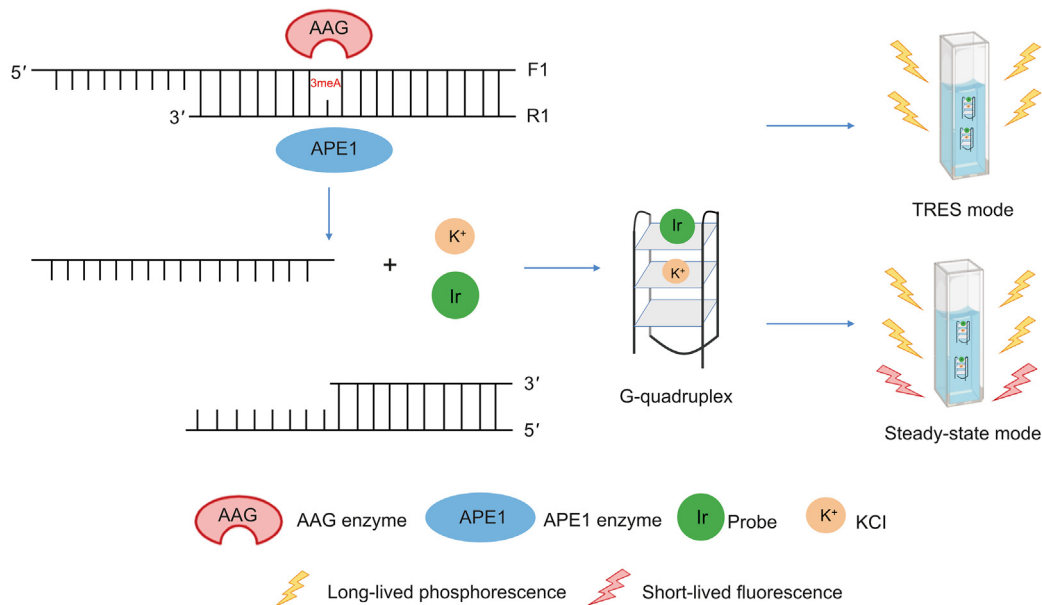


Fig. 1. Diagram for screening new alkyladenine DNA glycosylase (AAG) inhibitors. APE1: apurinic/aprimidinic endonuclease 1; 3meA: N3-methyladenine; Ir: Iridium; TRES: time-resolved emission spectroscopy.

3.2. Comparison of TRES with steady-state methods to screen AAG inhibitors

Circular dichroism (CD) spectroscopy was used to verify the formation of the F1 G-quadruplex structure. CD spectroscopy of the

F1 G-quadruplex-forming fragment showed a 266 nm strong positive peak and a 220 nm weaker negative peak, which is a G-quadruplex of the hybrid type [19] (Fig. S2). The selectivity of the G-quadruplex-specific iridium (III) probe for G-quadruplex DNA was then evaluated. Probe emission was evaluated in the presence

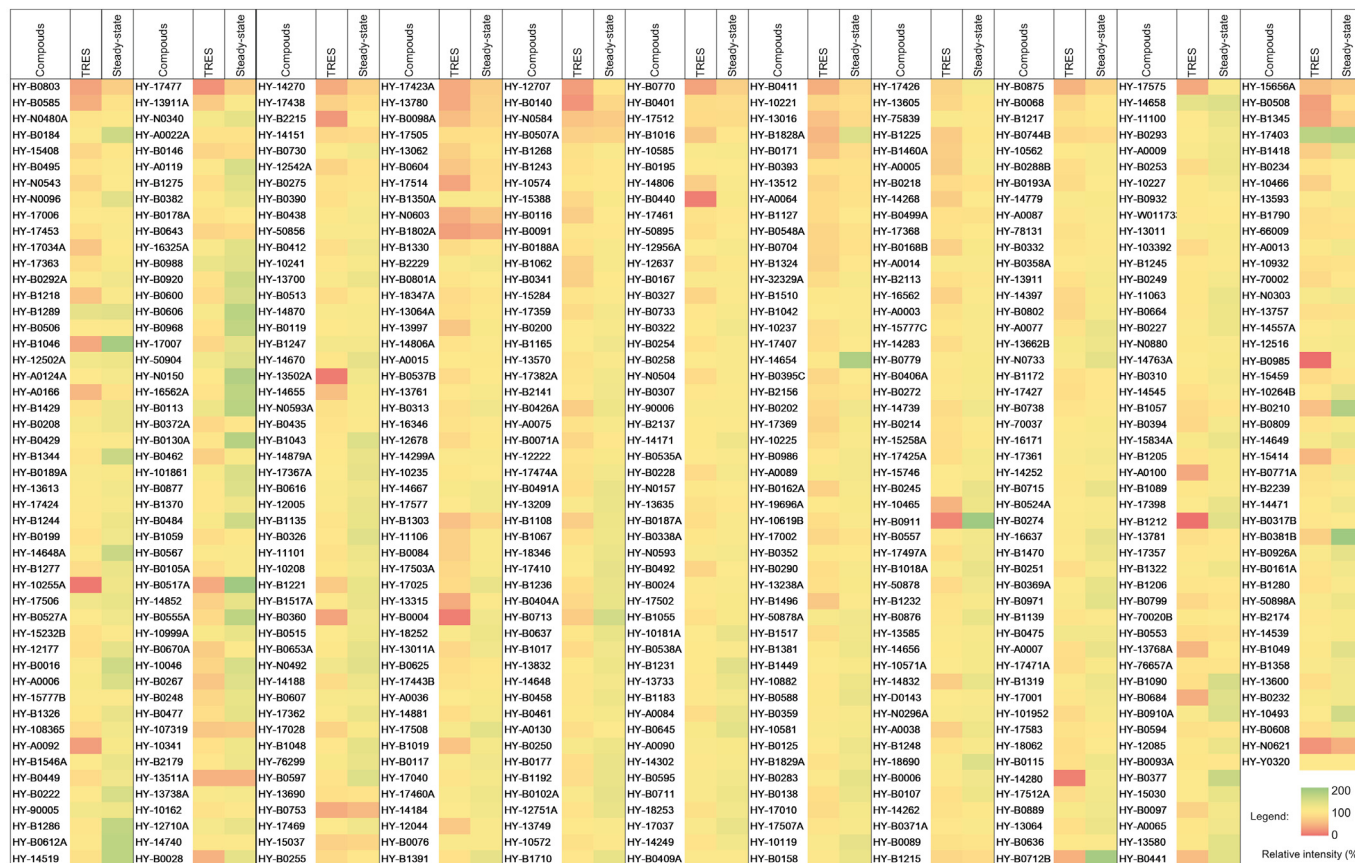


Fig. 2. Alkyladenine DNA glycosylase (AAG) inhibitor screening in a US Food and Drug Administration (FDA)-approved library by time-resolved emission spectroscopy (TRES) or steady-state methods. A lower relative intensity value, indicated by a color that appears closer to orange-red on the color scale, is suggestive of the presence of AAG inhibitors.

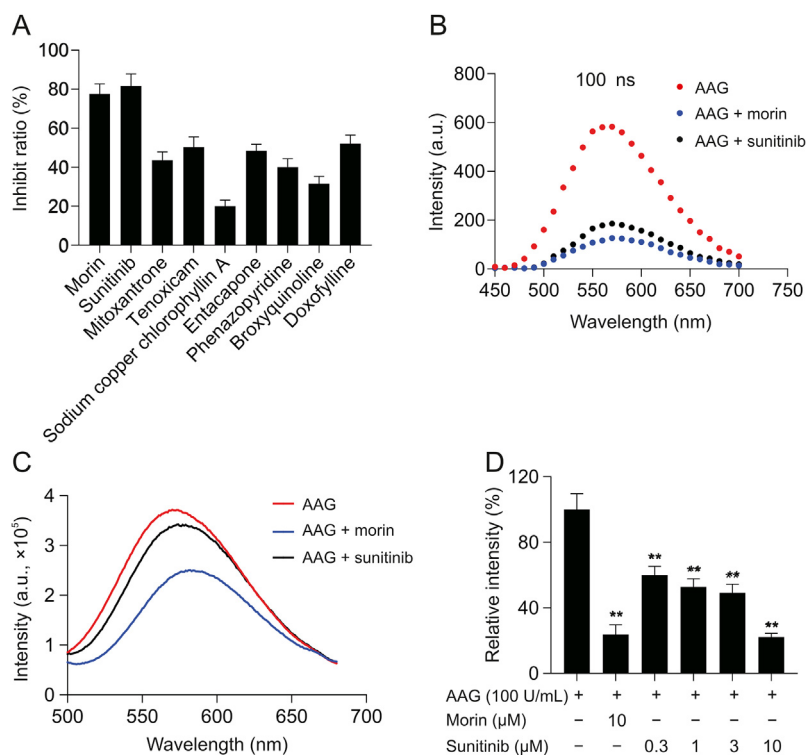


Fig. 3. Screening method based on time-resolved emission spectroscopy (TRES) could successfully prevent false negatives. (A) Alkyladenine DNA glycosylase (AAG) inhibition of eight potential US Food and Drug Administration (FDA)-approved drugs as measured by TRES. The inhibit ratio was calculated by the percentage reduction of emission of the probe compared to dimethyl sulfoxide (DMSO). (B) TRES mode or (C) steady-state emission spectra of the probe with AAG (100 U/mL), AAG (100 U/mL) + 10 μ M morin, or AAG (100 U/mL) + 10 μ M sunitinib. With excitation at 355 nm, the intensity of the luminescence emission was measured between 450 and 700 nm. (D) Sunitinib's dosage effect on AAG activity as studied by TRES method. *P* values were calculated using a two-sided *t*-test. ***P* < 0.01 compared with DMSO group.

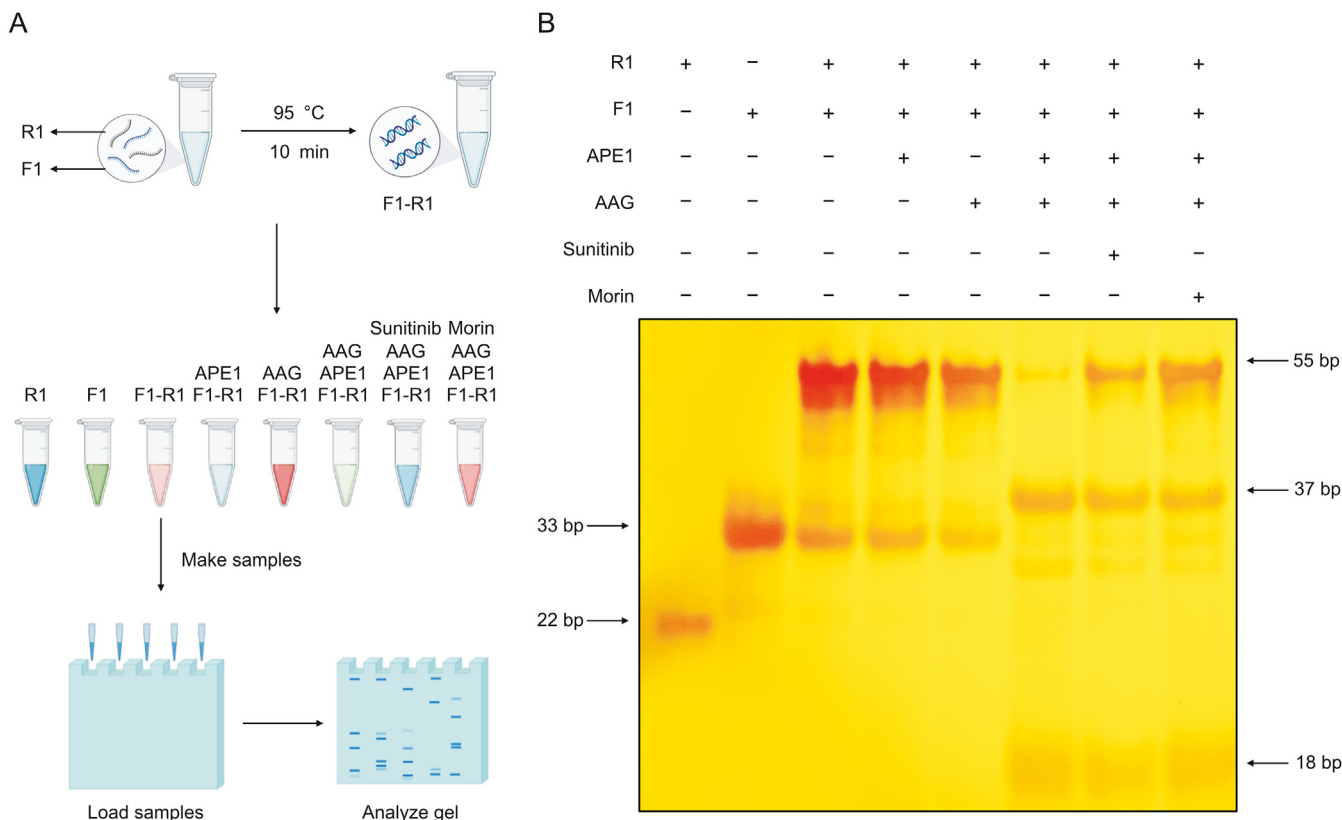


Fig. 4. Sunitinib could inhibit the activity of alkyladenine DNA glycosylase (AAG). (A) Preparation of samples. (B) DNA assay reaction products were subjected to polyacrylamide gel electrophoresis analysis and silver staining regardless of the presence of sunitinib or morin. APE1: apurinic/aprymidinic endodeoxyribonuclease 1.

of several types of DNA (Table S1). Upon incubation with G-quadruplex PS2.M, the probe exhibited the most significant increase in emission, followed by c-kit87up, c-kit1, Pu22, Grich, and c-kit2 G-quadruplexes (Fig. S3A). No significant difference was observed in luminescence when the probe was incubated with ssDNA or dsDNA. Therefore, the PS2.M sequence forms a suitable G-quadruplex structure for our probe and was therefore used for the design of the F1 strand. Consistent with this, the iridium (III) probe showed markedly increased emission with the G-quadruplex DNA sequence F1, whereas R1 or single-stranded DNA only showed slight changes in luminescence (Fig. S3B). In summary, the probe can function as a signal transducer when a quadruplex scaffold is produced from an ssDNA or dsDNA substrate because of the selective recognition of the G-quadruplex motif, resulting in an increased emission signal.

The experimental conditions for the sensing were optimized. The system displayed the highest emission response at a probe concentration of 1 μM , pH 7.0, and K^+ concentration of 25 mM (Fig. S4). The platform was used to screen a database of 1440 US FDA-approved drug compounds (10 μM) for AAG inhibition. However, under steady-state screening conditions, compared with the DMSO group (HY-Y0320), nearly every prepared sample demonstrated stronger emission responses due to the intrinsic fluorescence of the drug molecules (Fig. 2). Consequently, the reduction in

luminescence of the iridium (III) probe was difficult to distinguish, even when AAG was inhibited, resulting in false-negative results. Therefore, we hypothesized that we could leverage the extended phosphorescence lifetime of the probe to screen the library using TRES, thereby circumventing any interference caused by the samples' short-lived fluorescence. The luminescence lifetime of the probe was over 1000 ns, which is more than 10 times longer than the lifetimes of US FDA-approved compounds, which were generally less than 100 ns (Fig. S5). Of the 1440 US FDA-approved drugs (Fig. S6), 531 compounds were found to significantly reduce the fluorescence intensity of the probe in TRES mode (Fig. 2). Among these, eight compounds (sunitinib, mitoxantrone, tenoxicam, sodium copper chlorophyllin A, entacapone, phenazopyridine, broxyquinoline, and doxofylline) were identified as potential AAG inhibitors. Moreover, two natural compound libraries purchased from Push Biotechnology (Chengdu, China) were screened using the TRES method (Figs. S7A and B). Several additional potential AAG inhibitors were also identified, including anethole trithione, a bile secretion-stimulating drug with relatively high AAG inhibitory activity (Figs. S7C and D). A silver-staining assay was performed to demonstrate the inhibitory effect of anethole trithione on AAG (Fig. S8). Lanes 1–5 (isolated oligonucleotides F1 or R1, F1-R1 duplex, F1-R1 duplex with APE1 alone, or with AAG enzyme, respectively) were consistent with the results of sunitinib. The

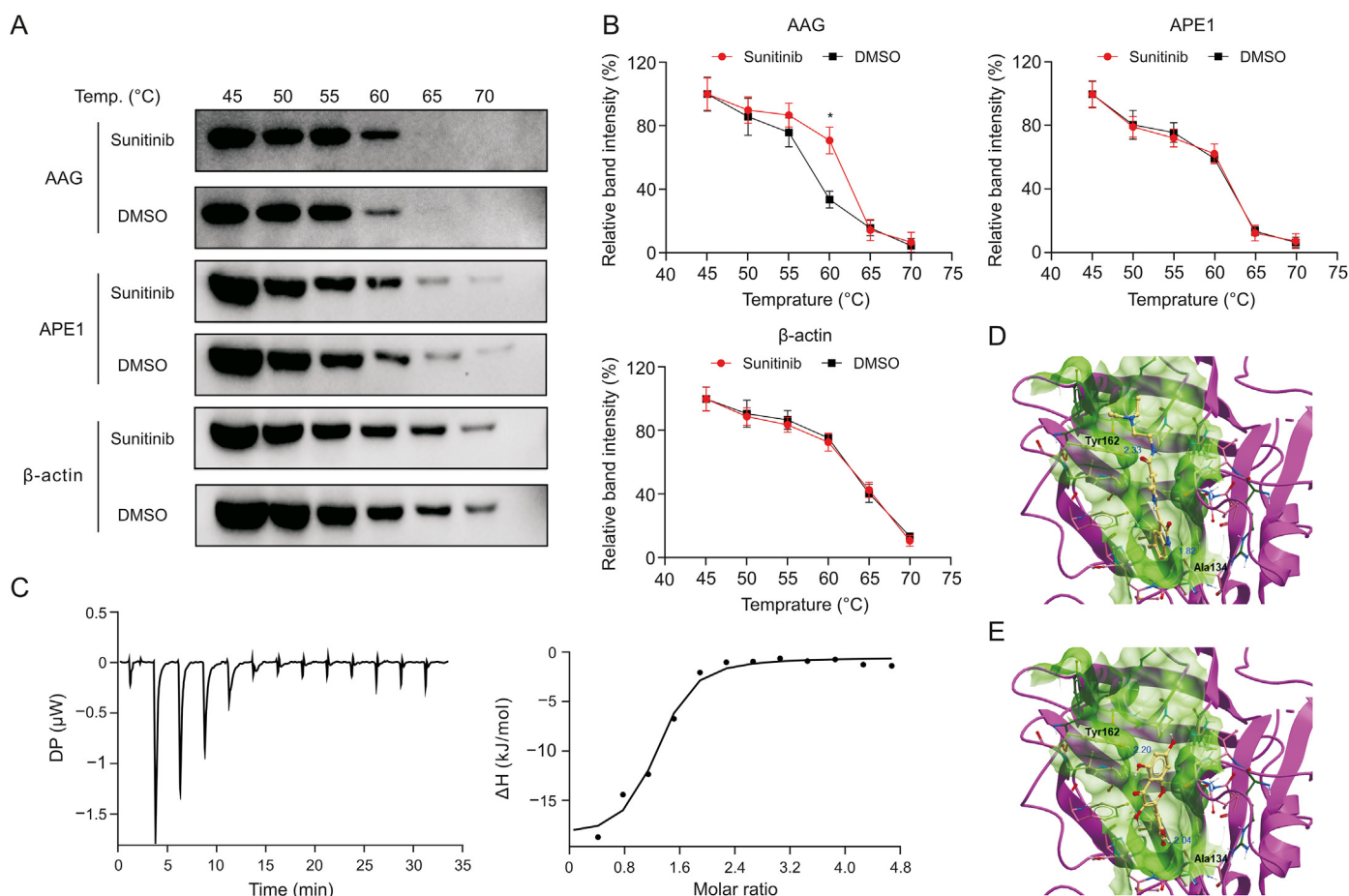


Fig. 5. Sunitinib engages alkyladenine DNA glycosylase (AAG). (A) Stabilization of AAG, apurinic/aprimidinic endodeoxyribonuclease 1 (APE1) or β -actin by sunitinib in cellulo. 10 μM sunitinib or dimethyl sulfoxide (DMSO) was added to T98G cell lysates for 30 min at 37 $^{\circ}\text{C}$, followed by 8 min of heating at various temperatures between 45 and 70 $^{\circ}\text{C}$. Protein sample supernatants were collected and identified using Western blotting. (B) AAG, APE1 or β -actin content in the soluble fraction by densitometry analysis. * $P < 0.05$ by t -test in comparison to DMSO group. (C) Isothermal titration calorimetric titration of sunitinib (500 μM) into recombinant AAG protein (20 μM). (D, E) The docking diagram of human AAG complexed with sunitinib (D) and morin (E) based on the X-ray crystal structure of human AAG complexed with N^6 -ethenoadenine DNA (PDB: 1EWN) using the internal coordinate mechanics (ICM) method. DP: differential power.

addition of anethole trithione (lane 6) prevented 3meA on F1 from being excised, even in the presence of both AAG and APE1. In contrast, in lane 7 (absence of anethole trithione), 3meA on F1 was excised by the action of AAG and APE1 to release R1 and cleaved F1. Moreover, addition of the positive control morin (lane 8) significantly suppressed this event. These results support the hypothesis that anethole trithione reduces the luminescence intensity of the G-quadruplex probe system in the TRES screen by suppressing AAG activity. Overall, the combined results demonstrated that the developed TRES screening assay is a very effective screening platform for AAG inhibitors and suitable for large-scale screening in the future. Overall, the results indicate that the TRES screening technique can efficiently overcome the issue of background fluorescence, thereby avoiding false-negatives.

Among the eight potential AAG inhibitors, sunitinib showed the highest AAG inhibition (Fig. 3A). The receptor tyrosine kinase inhibitor sunitinib is used to treat gastrointestinal stromal tumors resistant to imatinib and renal cell carcinoma. Owing to the long-lived luminescence lifetime of the probe, the inhibition of AAG activity by sunitinib could be easily detected in the TRES mode (Fig. 3B). In contrast, sunitinib showed no apparent inhibition in the steady-state mode owing to its high intrinsic fluorescence; hence, it was recorded as a false negative (Fig. 3C). A dose-response experiment further confirmed the AAG inhibitory activity of sunitinib, which showed even greater inhibition of AAG activity (81.2% at 10 μ M) compared to the positive control morin (77.5%) [34]

(Fig. 3D). These results indicated that sunitinib could be an effective AAG inhibitor screened using the TRES method.

3.3. Sunitinib inhibited AAG activity by DNA polyacrylamide gel electrophoresis

To verify the inhibitory activity of sunitinib on AAG, non-denaturing polyacrylamide gel electrophoresis was employed (Supplementary data and Fig. 4). Isolated F1 and R1 oligonucleotides migrate more quickly on the gel (lanes 1 and 2), compared to the F1-R1 duplex (lane 3). Neither APE1 (lane 4) nor AAG (lane 5) could solely liberate the G-quadruplex fragment. 3meA on F1 was excised in the presence of both AAG and APE1 to release R1 and cleaved F1 (lane 6). However, the addition of either sunitinib (lane 7) or the positive control morin (lane 8) suppressed this effect. These findings demonstrate that, as opposed to other mechanisms, such as emission quenching, the reduction in luminescence intensity of the G-quadruplex-probe system by sunitinib is likely caused by the suppression of AAG activity.

3.4. Stability enhancement of AAG in vitro and in cellulo through sunitinib

A cellular thermal shift assay (Supplementary data) was used to investigate whether sunitinib targets AAG to achieve its effects. In sunitinib-treated T98G cell lysates, clear shifts in the melting

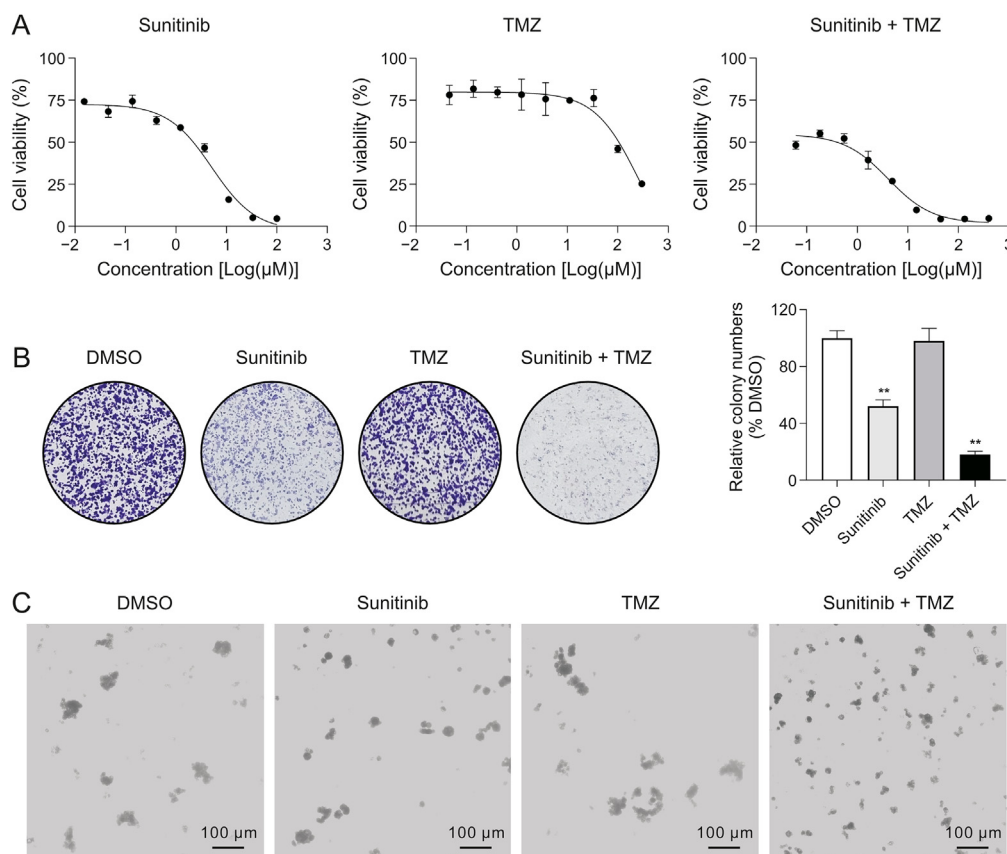


Fig. 6. Sunitinib/temozolomide (TMZ)/combination therapy inhibited glioblastoma (GBM) cell proliferation and stemness by targeting alkyladenine DNA glycosylase (AAG). (A) Cytotoxicity effect of sunitinib/TMZ/combination therapy on T98G cells. The cytotoxicity of the cells was assessed using the 3-(4,5-dimethyl-2-thiazolyl)-2,5-diphenyl-2-*H*-tetrazolium bromide (MTT) after 72 h of treatment with the indicated concentrations of sunitinib/TMZ/combination therapy. (B) T98G cell proliferation was inhibited by sunitinib/TMZ/combination therapy through the colony formation assay. (C) Sunitinib/TMZ/combination therapy inhibited T98G 3D cell sphere formation. The data are shown as mean \pm standard deviation (SD). ** $P < 0.01$ vs. dimethyl sulfoxide (DMSO) group.

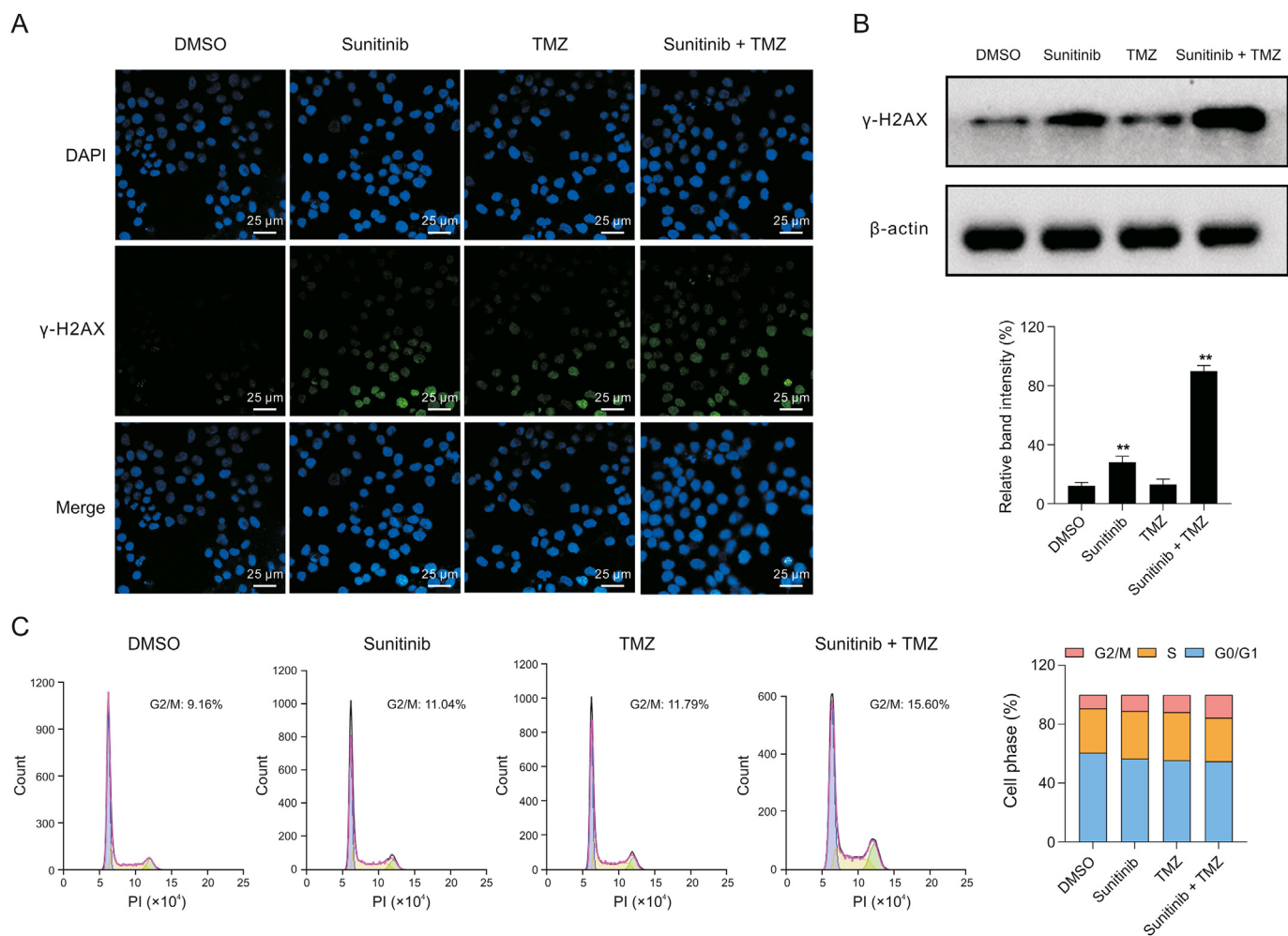


Fig. 7. Sunitinib and temozolomide (TMZ) treatment enhanced cycle arrest and DNA damage in T98G GBM cells. (A) T98G cells were treated with dimethyl sulfoxide (DMSO), sunitinib (3 μ M), TMZ (10 μ M), and the combination group for 24 h and visualized using a confocal laser scanning microscope. (B) DMSO, 3 μ M sunitinib, 10 μ M TMZ, and the combination group were used to treat T98G cells for 24 h before the expression of γ -H2AX and β -actin proteins was examined using Western blotting with quantification using densitometry. (C) Cell cycle assay with compound sunitinib, TMZ, or combination on T98G cells. DMSO, 3 μ M sunitinib, 10 μ M TMZ, and the combination group were treated to T98G cells for 24 h, respectively. The distribution of cells in the G0/G1, S, and G2/M phases is then calculated as a percentage. ** $P < 0.01$ vs. dimethyl sulfoxide (DMSO) group. DAPI: 4',6-diamidino-2-phenylindole; PI: propidium iodide.

temperature of AAG were observed (Figs. 5A and B). However, sunitinib had no obvious effect on the thermal stability of APE1 or β -actin. This suggests that sunitinib directly engages and stabilizes AAG even in the presence of complicated cellular debris. To further explore the thermodynamic parameters of the interaction between sunitinib and AAG, isothermal titration calorimetric (Supplementary data) was performed (Fig. 5C). The stoichiometry of the interaction was determined to be $N = 1.15 \pm 0.06$, indicating the presence of one sunitinib-binding site in AAG. Sunitinib and AAG possessed an endothermic interaction ($\Delta H = 18.4 \pm 1.51$ kcal/mol), and a favorable entropic contribution ($-T\Delta S = +15.6$ kcal/mol) was compensated. The K_D value was determined to be 1.14 ± 0.55 μ M. In addition, to further verify the feasibility of our assay, the X-ray crystal structure of human AAG complexed with N^6 -ethenoadenine DNA (PDB:1EWN) [35,36] was used as a molecular model (Supplementary data) for virtual screening using the internal coordinate mechanics (ICM) method (ICM-Pro 3.9-1b program; Molsoft, San Diego, CA, USA). First, the positive control morin was docked against the enzyme active site of AAG and was predicted to form two hydrogen bonds involving tyrosine 163 and alanine 34 with a high binding score of -17.18 . The identified compound sunitinib also displayed a similar binding mode with a

comparative score of -15.13 . This result supported the hypothesis that sunitinib acts by targeting AAG in the TRES assay.

3.5. Inhibition of AAG activity inhibits cell proliferation and cancer stem cell ability of GBM

However, the therapeutic potency of numerous antitumor agents is hindered by their side effects on healthy tissues. Combination therapy can potentially increase efficacy and decrease toxicity by allowing the use of anticancer agents at lower concentrations. As AAG depletion sensitized GBM cells to TMZ, the ability of sunitinib to synergize with TMZ was explored. The proliferation of T98G glioblastoma cells was measured using the 3-(4,5-dimethyl-2-thiazolyl)-2,5-diphenyl-2-*H*-tetrazolium bromide (Supplementary data) in the presence of sunitinib, TMZ, or their combination (Fig. 6A). The IC_{50} of sunitinib against T98G cells was 3 μ M, whereas TMZ alone showed no obvious antiproliferative activity ($IC_{50} > 100$ μ M). Interestingly, the combination of sunitinib and TMZ exhibited IC_{50} of 0.1 μ M. The combination index between sunitinib and TMZ was < 1 , suggesting synergism between these two compounds (Table S2). The colony formation experiment (Supplementary data) also indicated that the combination therapy

could significantly suppress T98G cell proliferation (Fig. 6B).

Cancer stem cells (CSC) are the main cause of cancer drug resistance. Our hypothesis suggests that the combination therapy of sunitinib and TMZ could potentially be effective against the characteristics of GBM CSC cells, despite their resistance to TMZ. Three-dimensional (3D) tumor spheres exhibit CSC characteristics, including high self-renewal ability, differentiation, and metastasis [37]. Therefore, the influence of combination therapy using sunitinib and TMZ on spheroid formation and the capacity of tumor sphere cells to self-renew was investigated using a 3D cell culture assay (Supplementary data). Spheroid formation was induced in T98G cells by seeding them in low-cell attachment dishes and then treating them for 2 weeks with 3 μ M sunitinib, 10 μ M TMZ, or a combination of both. As shown in Fig. 6C, the combination therapy suppressed T98G 3D cell growth with superior potency compared to sunitinib or TMZ alone.

3.6. Inhibition of AAG activity promotes DNA damage and cell cycle arrest in GBM

The comet assay (Supplementary data) was performed to detect DNA damage by 3.0 μ M sunitinib, 10 μ M TMZ, or their combination in T98G cells. The results showed that the length of the tail and the percentage of cells with a long tail increased in the combination group, demonstrating the DNA damage-inducing effect of the sunitinib and TMZ combination (Fig. S9). Importantly, compared to the control group or single-treatment groups, the combination group had greater efficacy in inducing DNA damage. The level of γ -H2AX, a sensitive DNA damage response marker, was determined using immunofluorescence staining (Supplementary data) and Western blotting (Supplementary data). As shown in Fig. 7A, γ -H2AX levels were markedly elevated following treatment with the combination group, and the effects of the combination were greater than those of the single treatment groups. In addition, Western blotting results showed that γ -H2AX expression was significantly increased in the co-treated group compared to that in the sunitinib or TMZ alone group (Fig. 7B). These findings suggest that the combined treatment of sunitinib and TMZ can significantly increase the level of DNA damage in T98G cells. DNA damage influences cell cycle progression. To further understand the impact of sunitinib and TMZ on cellular proliferation, a cell cycle analysis was conducted (Supplementary data). As shown in Fig. 7C, sunitinib or TMZ treatment partially induced cell cycle arrest at the G2/M phase in T98G cells. Compared to the use of either sunitinib or TMZ alone, the combination of these two agents resulted in a significant increase in G2/M phase cell cycle arrest. Based on the findings from the aforementioned experiments, it can be inferred that the combined use of sunitinib and TMZ has the potential to induce cell cycle arrest in GBM cells, thereby leading to a therapeutic effect in the treatment of cancer.

4. Conclusion

In summary, we established a TRES method for the detection of AAG inhibitor activity while circumventing the interference caused by the fluorescence background of the samples. This study repurposed an US FDA-approved drug, sunitinib, as a new AAG inhibitor. Moreover, sunitinib exhibited synergism with TMZ in triggering DNA damage and slowing the growth of GBM cells. Significantly, there are known anticancer properties of sunitinib that have been documented in scientific literature, and the discovery that sunitinib can inhibit AAG activity may potentially expedite the repurposing of existing drugs as a strategy to combat anticancer resistance conferred by specific targets. We anticipate that the effective screening method will be easily modified for screening additional

DNA repair enzyme inhibitors for potential therapeutic applications, including previously disregarded scaffold types that could not be screened owing to their high intrinsic fluorescence, leading to false negatives.

CRediT author statement

Ying-Qi Song: Methodology, Validation, Writing - Original draft preparation, Conceptualization; **Guo-Dong Li, Dou Niu, and Feng Chen:** Validation, Methodology, Formal analysis; **Shaozhen Jing:** Software, Formal analysis; **Vincent Kam Wai Wong:** Resources, Methodology; **Wanhe Wang:** Resources, Conceptualization, Funding acquisition; **Chung-Hang Leung:** Supervision, Project administration, Funding acquisition, Conceptualization, Writing - Reviewing and Editing.

Declaration of competing interest

The authors declare that there are no conflicts of interest.

Acknowledgments

This work is supported by the Science and Technology Development Fund (Grant Nos.: 0007/2020/A1 and 0020/2022/A1), the State Key Laboratory of Quality Research in Chinese Medicine, University of Macau (Grant No.: SKL-QRCM(UM)-2020-2022), the University of Macau (Grant Nos.: MYRG2019-00002-ICMS and MYRG2020-00017-ICMS), 2022 Internal Research Grant of SKLQRCM (University of Macau) (Grant No.: QRCM-IRG2022-011), the National Natural Science Foundation of China (Grant No.: 22101230), the Natural Science Basic Research Program of Shaanxi (Grant No.: 2021JQ-089), and the Natural Science Foundation of Chongqing, China (Grant No.: cstc2021jcyj-msxmX0659).

Appendix A. Supplementary data

Supplementary data to this article can be found online at <https://doi.org/10.1016/j.jppha.2023.04.010>.

References

- [1] C.H. Fan, W.L. Liu, H. Cao, et al., O⁶-methylguanine DNA methyltransferase as a promising target for the treatment of temozolomide-resistant gliomas, *Cell Death Dis.* 4 (2013), e876.
- [2] D. Fu, J.A. Calvo, L.D. Samson, Balancing repair and tolerance of DNA damage caused by alkylating agents, *Nat. Rev. Cancer* 12 (2012) 104–120.
- [3] S.Y. Lee, Temozolomide resistance in glioblastoma multiforme, *Genes Dis.* 3 (2016) 198–210.
- [4] E. Mas Claret, B. Al Yahyaee, S. Chu, et al., An aza-nucleoside, fragment-like inhibitor of the DNA repair enzyme alkyladenine glycosylase (AAG), *Bioorg. Med. Chem.* 28 (2020), 115507.
- [5] J. Paik, T. Duncan, T. Lindahl, et al., Sensitization of human carcinoma cells to alkylating agents by small interfering RNA suppression of 3-alkyladenine-DNA glycosylase, *Cancer Res.* 65 (2005) 10472–10477.
- [6] P.A.J. Crosbie, A.J. Watson, R. Agius, et al., Elevated N3-methylpurine-DNA glycosylase DNA repair activity is associated with lung cancer, *Mutat. Res.* 732 (2012) 43–46.
- [7] L.J. Hofseth, M.A. Khan, M. Ambrose, et al., The adaptive imbalance in base excision-repair enzymes generates microsatellite instability in chronic inflammation, *J. Clin. Invest.* 112 (2003) 1887–1894.
- [8] C. Liu, Y. Tu, J. Yuan, et al., Aberrant expression of N-methylpurine-DNA glycosylase influences patient survival in malignant gliomas, *J. Biomed. Biotechnol.* 2012 (2012), 760679.
- [9] G. Serrano-Heras, B. Castro-Robles, C.M. Romero-Sánchez, et al., Involvement of N-methylpurine DNA glycosylase in resistance to temozolomide in patient-derived glioma cells, *Sci. Rep.* 10 (2020), 22185.
- [10] S. Agnihotri, A.S. Gajadhar, C. Ternamian, et al., Alkylpurine-DNA-N-glycosylase confers resistance to temozolomide in xenograft models of glioblastoma multiforme and is associated with poor survival in patients, *J. Clin. Invest.* 122 (2012) 253–266.
- [11] P. Wang, A.B. Guliaev, B. Hang, Metal inhibition of human N-methylpurine-DNA glycosylase activity in base excision repair, *Toxicol. Lett.* 166 (2006)

- 237–247.
- [12] M. Cristóvão, E. Sisamakís, M.M. Hingorani, et al., Single-molecule multiparameter fluorescence spectroscopy reveals directional MutS binding to mismatched bases in DNA, *Nucleic Acids Res.* 40 (2012) 5448–5464.
- [13] A. Romani, C. Clementi, C. Miliani, et al., Fluorescence spectroscopy: A powerful technique for the noninvasive characterization of artwork, *Acc. Chem. Res.* 43 (2010) 837–846.
- [14] S. Lin, W. Gao, Z. Tian, et al., Luminescence switch-on detection of protein tyrosine kinase-7 using a G-quadruplex-selective probe, *Chem. Sci.* 6 (2015) 4284–4290.
- [15] A. Ruggi, F.W.B. van Leeuwen, A.H. Velders, Interaction of dioxygen with the electronic excited state of Ir(III) and Ru(II) complexes: principles and biomedical applications, *Coord. Chem. Rev.* 255 (2011) 2542–2554.
- [16] S. Lin, L. Lu, T.S. Kang, et al., Interaction of an iridium(III) complex with G-quadruplex DNA and its application in luminescent switch-on detection of siglec-5, *Anal. Chem.* 88 (2016) 10290–10295.
- [17] K.H. Leung, H.-Z. He, B. He, et al., Label-free luminescence switch-on detection of hepatitis C virus NS3 helicase activity using a G-quadruplex-selective probe, *Chem. Sci.* 6 (2015) 2166–2171.
- [18] E. Babu, J. Bhuvanewari, K. Rajakumar, et al., Non-conventional photoactive transition metal complexes that mediated sensing and inhibition of amyloidogenic aggregates, *Coord. Chem. Rev.* 428 (2021), 213612.
- [19] G. Li, S.A. Henry, H. Liu, et al., A robust photoluminescence screening assay identifies uracil-DNA glycosylase inhibitors against prostate cancer, *Chem. Sci.* 11 (2020) 1750–1760.
- [20] S. Lin, T.-S. Kang, L. Lu, et al., A G-quadruplex-selective luminescent probe with an anchor tail for the switch-on detection of thymine DNA glycosylase activity, *Biosens. Bioelectron.* 86 (2016) 849–857.
- [21] L. Lu, Z. Mao, T.-S. Kang, et al., A versatile nanomachine for the sensitive detection of platelet-derived growth factor-BB utilizing a G-quadruplex-selective iridium(III) complex, *Biosens. Bioelectron.* 85 (2016) 300–309.
- [22] S. Neidle, G.N. Parkinson, The structure of telomeric DNA, *Curr. Opin. Struct. Biol.* 13 (2003) 275–283.
- [23] X.-X. Huang, L.-N. Zhu, B. Wu, et al., Two cationic porphyrin isomers showing different multimeric G-quadruplex recognition specificity against monomeric G-quadruplexes, *Nucleic Acids Res.* 42 (2014) 8719–8731.
- [24] Y. Cui, D. Kong, C. Ghimire, et al., Mutually exclusive formation of G-quadruplex and i-motif is a general phenomenon governed by steric hindrance in duplex DNA, *Biochemistry* 55 (2016) 2291–2299.
- [25] L. Deng, X. Ouyang, J. Jin, et al., Exploiting the higher specificity of silver amalgamation: selective detection of mercury(II) by forming Ag/Hg amalgam, *Anal. Chem.* 85 (2013) 8594–8600.
- [26] Z. Chen, Y. Lin, C. Zhao, et al., Silver metallization engineered conformational switch of G-quadruplex for fluorescence turn-on detection of biothiols, *Chem. Commun.* 48 (2012) 11428–11430.
- [27] H. Xu, S. Gao, Q. Yang, et al., Amplified fluorescent recognition of g-quadruplex folding with a cationic conjugated polymer and DNA intercalator, *ACS Appl. Mater. Interfaces* 2 (2010) 3211–3216.
- [28] K.-H. Leung, H.-Z. He, B. He, et al., Label-free luminescence switch-on detection of hepatitis C virus NS3 helicase activity using a G-quadruplex-selective probe, *Chem. Sci.* 6 (2015) 2166–2171.
- [29] D.L. Ma, C. Wu, Z.-Z. Dong, et al., The development of G-quadruplex-based assays for the detection of small molecules and toxic substances, *Chem. Asian J.* 12 (2017) 1851–1860.
- [30] Z.-Z. Dong, L. Lu, W. Wang, et al., Luminescent detection of nicking endonuclease Nb.BsmI activity by using a G-quadruplex-selective iridium(III) complex in aqueous solution, *Sensor. Actuator. B Chem.* 246 (2017) 826–832.
- [31] D. Sun, Y. Liu, D. Liu, et al., Stabilization of G-quadruplex DNA, inhibition of telomerase activity and live cell imaging studies of chiral ruthenium(II) complexes, *Chemistry* 18 (2012) 4285–4295.
- [32] S.N. Georgiades, N.H. Abd Karim, K. Suntharalingam, et al., Interaction of metal complexes with G-quadruplex DNA, *Angew. Chem., Int. Ed. Engl.* 49 (2010) 4020–4034.
- [33] L. Lu, W. Wang, C. Yang, et al., Iridium(III) complexes with 1,10-phenanthroline-based N'N ligands as highly selective luminescent G-quadruplex probes and application for switch-on ribonuclease H detection, *J. Mater. Chem. B* 4 (2016) 6791–6796.
- [34] M. Dixon, J. Woodrick, S. Gupta, et al., Naturally occurring polyphenol, morin hydrate, inhibits enzymatic activity of N-methylpurine DNA glycosylase, a DNA repair enzyme with various roles in human disease, *Bioorg. Med. Chem.* 23 (2015) 1102–1111.
- [35] G.-J. Yang, W. Wang, P.M. Lei, et al., A 7-methoxybicycoumarin derivative selectively inhibits BRD4 BD2 for anti-melanoma therapy, *Int. J. Biol. Macromol.* 164 (2020) 3204–3220.
- [36] A.Y. Lau, M.D. Wyatt, B.J. Glassner, et al., Molecular basis for discriminating between normal and damaged bases by the human alkyladenine glycosylase, AAG, *Proc. Natl. Acad. Sci. U. S. A.* 97 (2000) 13573–13578.
- [37] S. Cheng, G.-J. Yang, W. Wang, et al., Discovery of a tetrahydroisoquinoline-based CDK9-cyclin T1 protein-protein interaction inhibitor as an anti-proliferative and anti-migration agent against triple-negative breast cancer cells, *Genes Dis* 9 (2022) 1674–1688.